

AD617105

U. S. Army Ordnance
Ballistic Research Laboratories
Aberdeen Proving Ground, Maryland
Approved Proposal No. 3175
Authorization No. 4086

①

EXPLOSIVES RESEARCH CENTER

| | | | | |
|------------|---|----|---|-----------|
| COPY | 1 | OF | 1 | 40 |
| HARD COPY | | | | \$. 2.00 |
| MICROFICHE | | | | \$. 0.50 |

37p



STRESS WAVES IN BOUNDED MEDIA

Quarterly Report
March 1, 1965 to May 31, 1965

BUREAU OF MINES, PITTSBURGH, PA.

UNITED STATES
DEPARTMENT OF
THE INTERIOR

④

STRESS WAVES IN BOUNDED MEDIA

Quarterly Report

March 1, 1965 to May 31, 1965

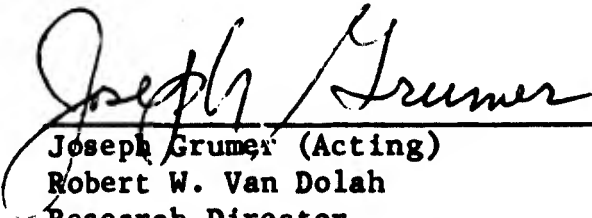
Prepared for:

**U. S. Army Ordnance
Ballistic Research Laboratories
Aberdeen Proving Ground, Maryland
Approved Proposal No. 3175
Authorization No. 4086**

by

**Richard W. Watson
Karl R. Becker
Frank C. Gibson**

Approved by:



**Joseph Grumer (Acting)
Robert W. Van Dolah
Research Director
Explosives Research Center**

**U. S. Department of the Interior
Bureau of Mines
Pittsburgh, Pa.
June 22, 1965**

STRESS WAVES IN BOUNDED MEDIA

Introduction

This is the second quarterly report of research conducted under a program entitled "Stress Waves in Bounded Media". The program is supported by the Ballistic Research Laboratories, Aberdeen Proving Ground, Maryland.

During the quarter, a shock-wave signature technique based on the 130-kilobar phase transition in Armco iron was explored. In addition, a spherical shock source to be used in shock reflection studies was developed and calibrated. The results of a detonation-rate study, using both liquid and solid explosive systems as well as some theoretical computations of the oblique collision of metallic liners, also appear in this report.

Techniques

A. Shock Signature Studies

During this quarter an experimental program was carried out in an attempt to develop a technique to define shock wave signatures based on the 130-kilobar phase transition characteristic of Armco iron. Fowler, Minshall, and Zukas^{1/} have shown that both micro and macrostructural differences in the crystalline structure as well as permanent density changes are observed in Armco specimens subjected to pressures above the transition pres-

^{1/} Fowler, C. M., F. S. Minshall, and E. G. Zukas. A Metallurgical Method for Simplifying the Determination of Hugoniot Curves for Iron Alloys in the Two-Wave Region. Response of Metals to High Velocity Deformation, Vol. 9, 275-308, Interscience Publishers, New York, 1960.

sure. Several practical applications of this technique suggest themselves; for example, it would serve as a tool in studying the reflection of shocks from the boundaries between two different materials and for exploring the coupling between a high-velocity projectile and a target as well as other applications. In our research it would be convenient if Armco samples having a minimum of metallurgical preparation could be used. In order to explore the possibility of using "as received" Armco iron, a series of tests were conducted using 1/2-inch thick x 4-inch diameter specimens cut from bar stock. Prior to the test firings the specimens were annealed for 1-1/2 hours at 700°C, then slowly cooled to room temperature. A photograph of a typical set-up is illustrated in figure 1. It consisted of an Armco sample which was shock loaded at five separate points using 3/4 x 3/4-inch tetryl donors in conjunction with shock attenuators having various thicknesses selected to induce pressures in the Armco, both above and below 130 kilobars. The attenuator thicknesses were selected on the basis of pressure calibration trials which will be discussed later. In addition, three different attenuator materials--aluminum, brass, and magnesium--were used in an effort to provide an unambiguous interpretation of the experimental results. After the test firings the Armco specimens were then lightly buffed with a fine grade steel wool and etched for 45 minutes in a solution of 60% water, 40% sulfuric acid, and 20% hydrochloric acid, by volume. Both the solution and the specimen were maintained at a temperature of 160°F throughout the etching period.

A photograph of a typical etched sample is presented in figure 2. In this case, aluminum attenuators having thicknesses ranging from 3/8 inch to 5/8 inch in 1/16-inch increments were used. As will be noted in figure 2, the areas which were shock

loaded with the $3/8$, $7/16$, and $1/2$ -inch attenuators indeed showed visual differences in appearance after the etching process. The shock-loaded areas corresponding to the $5/8$ and $9/16$ -inch thick attenuator had the same coloration as unloaded plate area which was generally a dull yellow, while the area corresponding to the $3/8$, $7/16$, and $1/2$ -inch attenuator revealed roughly circular areas which were usually dark gray in color. It is interesting to note that the diameter of the latter decrease with increasing attenuator thickness suggesting appreciable frontal curvature of the attenuator shock. If it is assumed that this difference is associated with the phase transition, it could be concluded that the critical thickness of attenuator required to produce the phase transition lies between $8/16$ and $9/16$ inch. In order to define this critical attenuator thickness more precisely, an additional series of tests were carried out with attenuators having thicknesses ranging from $15/32$ to $19/32$ of an inch in $1/32$ -inch increments. This same procedure was then carried out using magnesium and brass attenuators in order to define the critical thickness for all three attenuator materials. In these tests it was found that the critical thickness required to produce the difference in the etching characteristics was approximately $25/64$ of an inch for the brass attenuators, $31/64$ of an inch for the magnesium attenuators, and $35/64$ of an inch for the aluminum attenuators. If the macroscopic differences revealed by the etching technique truly represent the 130-kilobar phase transition in Armco iron, then these attenuator thicknesses and donor combinations should be just adequate to deliver a peak pressure of 130 kilobars to the Armco test specimens.

In order to deduce the pressures delivered to the Armco

test specimens, a series of independent pressure calibration trials were carried out using all three attenuator materials. The experimental arrangement used in these tests is illustrated in figure 3. It consisted of 3/4-inch x 3/4-inch tetryl donor and shock attenuators of the same diameter used in the experiments with the Armco samples. A 1/32-inch thick x 1/2-inch diameter wafer of the same material comprising the attenuator is affixed to the free surface of the attenuator using a very thin coat of vaseline. The average wafer velocity over a trajectory of roughly 5 inches was determined by means of a high-speed chronograph. Previous experiments have indicated that the wafer velocity can be taken as a very close approximation of the free surface velocity of the shock attenuator^{2/}. The results of these trials are presented in table 1 in terms of free surface velocity as a function of attenuator thickness. Time of flight values shown in table 1 have been corrected to take into account the time required for the shock wave to traverse the attenuator; the corrected values are also included. These results are summarized in figure 4 in terms of peak pressure as a function of attenuator thickness. From these data, the peak pressures in the attenuator at their critical thickness for producing changes in the Armco specimens are deduced to be 113 kilobars for brass, 79 kilobars for aluminum, and 67 kilobars for the magnesium. If the differences observed in the experiments with the Armco samples truly correspond to the 130-kilobar phase transition, then a plot of the reflected Hugoniot of the three attenuator materials in the particle velocity pressure plane should intersect at a common point representative of the pressure required to produce the phase transition. This construction is illustrated in figure 5

^{2/} Watson, R. W., K. R. Becker, and F. C. Gibson. Hypervelocity Impact Phenomena. Bureau of Mines Quarterly Report, U. S. Army Ordnance, Aberdeen Proving Ground, Md., September 1, 1963 to November 30, 1963.

together with the shock Hugoniot of Armco which is valid to 130 kilobars^{3/}. As will be observed, the results do indicate a common delivered pressure of roughly 120 kilobars. There is a certain "area of confusion" associated with this type of analysis which results from a lack of precision in the experimental data. While the common pressure is somewhat below the 130 kilobars quoted by other investigators^{4/}, it should be pointed out that the pressure calibration trials, as a result of integrating effects associated with the finite wafer thickness and air drag, tend to produce values of free surface velocity which are below the true surface velocity of the attenuators. As a consequence, each of the reflected Hugoniots shown in figure 5 could be shifted to the right along the particle velocity axis. This would tend to elevate the common intersection point and bring it more nearly into agreement with the 130-kilobar value quoted for the phase transition. In view of the anticipated value of this general technique, additional experiments are being carried out in an effort to define more precisely the pressures associated with the macroscopic differences observed in the Armco samples as well as a grade of mild steel.

B. Spherical Charge Development

An explosive shock source has been developed for future studies involving the reflection of spherical shocks from plane boundaries. The explosive assembly, illustrated in figure 6, consists of a two-inch diameter sphere of cast pentolite ($\rho = 1.61$) with a one-half inch diameter spherical cavity at its center. The

^{3/} Erkman, John O. Smooth Spalls and the Polymorphism of Iron. Poulter Laboratories Technical Report 012-60, Stanford Research Institute, Menlo Park, California, December 16, 1960 (pp. 29).

^{4/} Bancroft, Dennison, Eric L. Peterson, and Stanley Minshall. Polymorphism of Iron at High Pressure. Jour. of Applied Physics, Vol. 27, No. 3, March 1956, pp. 291-298.

cavity contains a more sensitive explosive (pressed PETN; $\rho = 0.7$) which is initiated by means of an electric discharge through a 3/32-inch gap located at the core of the charge. Electrical energy is provided by a capacitor discharge circuit (similar to those used in exploding wire systems). Energy stored in capacitors is triggered into the spark gap using a 5C22 thyratron as a switching device. The source energy is about 200 joules (12 kv; 3 μ f) and is conducted to the spark gap at the center of the explosive system by means of two small insulated electrodes having a diameter of 0.032 inch. The explosive assemblies were cast in two hemispherical sections with appropriate hemispherical cavities for the PETN and grooves for the electrode wires; they were then carefully fitted together and bonded.

Five of the spherical charge assemblies were tested for reproducible behavior by firing them under water; streak photography was used to determine shock velocity as a function of radial position measured from the surface of the charge. A sketch of the experimental set-up is shown in figure 7. The spherical charges were positioned in 8 inch x 8 inch x 6-inch deep Plexiglas water tanks with the axis of the electrodes in the vertical position; the slit of the camera was aligned through the center of the charge in the horizontal plane. The system was backlit by a light from an exploding wire with a circuit similar to that used to initiate the charge.

A streak photograph for one of the trials is presented in figure 8. The central portion of the photograph represents the space occupied by the charge or expanding explosive products and a shock may be observed traveling both to the left and right of this area. Both the left and right shock trajectories were analyzed for record.

The basic data obtained specify the radial position of the shock as a function of time. A further reduction of the data, using a mechanical differentiation technique, yielded shock velocity as a function of radial position. These data, for each individual shock trajectory, are tabulated in table 2. The average shock velocity as a function of radial position for all trajectories is plotted in figure 9. The limits of variation indicated by bars represent the maximum departure of any individual data set from the average.

The average shock velocity at 0.5 cm from the surface of the sphere is about 4.2 mm/ μ sec with a maximum deviation (as defined above) of about 0.5 mm/ μ sec; at 6.0 cm the shock velocity has attenuated to about 2.1 mm/ μ sec (which is still somewhat above the sound velocity in the fluid) and the variation between data sets is negligible; about 70% of the attenuation takes place between the 0.5-cm and 2.0-cm position interval.

The chief aim of this particular development program was to make available a spherical shock source with some reasonably precise knowledge of the peak pressures at various specified distances from the source. Hence, pressures corresponding to the shock velocities have been determined through the use of equation-of-state data for water published by Rice and Walsh^{5/}. The pressure vs position relationship is shown in figure 10. The pressure at a point 0.5 cm from the charge is about 60 kilobars; at 3 cm and 6 cm the pressures are about 11 and 5 kilobars, respectively. The results of this series of trials are in excellent agreement with results published by Cole^{6/} which are included for

^{5/} Rice, M. H. and J. M. Walsh. Equation of State of Water to 250 Kilobars. J. Chem. Phys., Vol. 26, No. 4, April 1957.

^{6/} Cole, Robert H. Underwater Explosions. Princeton University Press, Princeton, N.J., 1948, 437 pages.

comparison purposes in figures 4 and 5.

Detonation Rates of Several Explosives as a
Function of Charge Diameter

A program designed to provide accurate detonation-rate measurements for several explosives in various diameter sizes has been completed. These data are required for a future precision shaped-charge program using liquid explosives and other related studies. The explosives involved were cast TNT ($\rho = 1.57$); cast Pentolite ($\rho = 1.61$), cast Composition B ($\rho = 1.72$) and liquid nitroglycerin-ethylene glycol dinitrate (NG-EGDN, $\rho_o = 1.55$). The four diameter sizes were 0.237 inch, 0.514 inch, 0.984 inch and 2.023 inches. The explosive length was about 8 inches and all were lightly confined in glass tubing.

Detonation rate measurements were obtained by streak camera methods; the camera had previously been calibrated^{7/} by some rather meticulous shots with nitromethane, the results of which were then compared with similar data obtained by an electronic method by Campbell et al^{8/}; agreement was within 0.25%.

The recently obtained detonation rate data and other relevant information are tabulated in table 3. The number of trials and variation between trials are also indicated in the table. In general, the number of trials was two and individual detonation rates differ from the mean values by about 0.3%.

^{7/} Watson, R. W., K. R. Becker, and F. C. Gibson. *Stress Waves in Bounded Media*. Bureau of Mines Quarterly Report, U. S. Army Ordnance, Aberdeen Proving Ground, Md., December 1, 1964 to February 28, 1965.

^{8/} Campbell, A. W., M. E. Malin, T. J. Boyd, Jr., and J. A. Hull. *Precision Measurement of Detonation Velocities in Liquid and Solid Explosives*. *Rev. Sci. Instr.*, Vol. 27, No. 8, 567-574, August 1956.

The data in the table are plotted in figure 11 which shows the relationship between detonation rate and charge diameter for the four explosive substances tested.

The trials carried out with NG-EGDN yielded rates ranging from 7.50 to 7.54 mm/ μ sec, thus indicating no significant change in detonation rate over the range of diameters investigated.

The data for the three solid cast explosives (TNT, Composition B, and pentolite) do, however, show a rate-diameter dependence. For TNT the data are restricted to the 1-inch and 2-inch diameter sizes because the explosive failed to detonate in the 1/4-inch and 1/2-inch diameter charges. The detonation did not go to completion in the 1-inch diameter size when a 1-inch diameter x 1/2-inch long tetryl booster was used (Composition B and pentolite did detonate properly with this size booster). Two complete detonations were, however, realized with 1-inch diameter TNT when the booster length was doubled. The streak record showed some evidence of over-driving by the booster in the first several centimeters of detonation but a lower steady detonation was obtained shortly thereafter; the over-driven portion was, of course, not considered in determining the rate. The rates obtained for the 1-inch and 2-inch diameter sizes were respectively 6.85 and 6.97 mm/ μ sec.

The data for Composition B show substantial increases in detonation rate when the diameter is increased from 1/4 inch to 1/2 inch; thereafter, the increase is rather slight up to the 2-inch diameter size. The rates at 1/4- and 1/2-inch charge diameter are 7.36 and 7.83 mm/ μ sec (an increase of about 6-1/2% for a 1/4-inch charge diameter increase). For the 1-inch and 2-inch diameter charges, the rates are respectively 7.82 and 7.89 mm/ μ sec (about 0.9% increase for a 1-inch charge diameter in-

crease)--the latter increase, although small, is believed to be significant; the minimum diameter for an ideal detonation (a detonation independent of diameter) is in excess of 1 inch. Further increases in rate, however, are not expected for diameters in excess of 2 inches since a precise detonation velocity value from a much larger size Composition B charge (5-1/2" x 5-1/2" x 3") in studies by Duff and Houston^{9/} was 7.868 mm/ μ sec or within about 0.28% of the value reported here for the 2-inch diameter size.

The data for 50/50 pentolite show detonation rate increases similar in character to those observed for Composition B. The detonation rate increases from 7.16 to 7.40 mm/ μ sec (3.4%) when charge diameter goes from 1/4 to 1/2 inch and increases from 7.43 to 7.53 mm/ μ sec (1.3%) between the 1-inch and 2-inch diameter interval. The latter increase is again believed to be significant and the minimum diameter for ideal detonation is thought to lie between 1 and 2 inches.

Shock Wave Interactions

A series of calculations have been carried out to determine the limiting conditions for jet formation in the high-velocity collision of like materials for several materials of common interest. The method used to determine these limiting conditions was originally outlined in a paper by Walsh, Shreffler, and Willig^{10/} where they presented results for 24ST aluminum, mild steel,

^{9/} Duff, Russell and Edwin Houston. Measurement of the Chapman-Jouguet Pressure and Reaction Zone Length in a Detonating High Explosive. J. Chem. Phys., Vol. 23, No. 7, July 1955, pp. 1268-1273.

^{10/} Walsh, J. M., R. G. Shreffler, and F. J. Willig. Limiting Conditions for Jet Formation in High Velocity Collisions. J. Appl. Phys., Vol. 24, No. 3, March 1953.

lead, and yellow brass. More recently, Cowan and Holtzman^{11/} have published the results of similar studies for gold, copper, and nickel. The calculations made by Walsh and his associates were based on an equation of state derived from an extrapolation of Bridgman's data using a theoretical equation of state for the high pressure end^{12/}. For this reason, as well as the fact that other materials are of specific interest in programs currently being carried out at the Bureau, the Ballistic Research Laboratories, and the Firestone Tire & Rubber Co., it seemed advisable to consider these and other materials using more recent experimental equation-of-state data. Calculations of this type are of further value since, in addition to indicating the conditions required to produce jetting in the collision of two materials, they also furnish valuable data relative to the state of the material behind the collision point. While a calculation of this type does not yield any specific information concerning, for example, the temperatures associated with jetted material, they do serve to set the lower limits for these parameters and also to broaden one's insight into these and other areas of immediate practical concern. In addition, the calculations establish useful guide lines for approaching such problems as the collision of more complex liner systems.

The flow configuration under consideration is depicted in figure 12 and is referred to a coordinate system moving with the point of collision M. For certain values of the initial flow velocity, U_0 , the deflection, θ , can be accomplished by a

^{11/} Cowan, G. R. and A. H. Holtzman. Flow Configurations in Colliding Plates: Explosive Bonding. J. Appl. Phys., Vol. 34, No. 4 (Part I), April 1963.

^{12/} Feynman, Metropolis, and Teller. Phys. Rev. 75, 1561 (1949).

single shock wave attached to the collision point. If U_o is held constant and ϕ is increased, a critical angle ϕ_c is reached where the flow configuration is no longer possible. For values of ϕ less than ϕ_c we have from the mechanical shock relations:

$$\rho_o U_{on} = \rho U_n \quad \text{conservation of mass} \quad (1)$$

$$P = \rho_o U_{on} (U_{on} - U_n) \quad \text{conservation of momentum} \quad (2)$$

perpendicular to shock front

$$U_{ot} = U_t \quad \text{conservation of momentum} \quad (3)$$

parallel to shock front

where ρ_o , U_{on} , and U_{ot} are the initial density, and the normal and tangential components of flow velocity relative to the shock front respectively, while ρ , U_n , U_t represent the values of these variables behind the shock front.

Equations (1) and (2) can be rewritten in terms of the normal velocity components as:

$$U_{on} = \left[\frac{P(\mu + 1)}{\rho_o \mu} \right]^{1/2} \quad (4)$$

$$U_n = \left[\frac{P}{\rho_o \mu (\mu + 1)} \right]^{1/2} \quad (5)$$

where μ is defined by:

$$\mu = \frac{\rho}{\rho_o} - 1. \quad (6)$$

An inspection of figure yields the following relationships:

$$U_{ot} = U_t = \left(U_o^2 - U_{on}^2 \right)^{1/2} \quad (7)$$

$$U = \left(U_t^2 + U_n^2 \right)^{1/2} \quad (8)$$

$$\phi = \tan^{-1} \frac{U_{on}}{U_t} - \tan^{-1} \frac{U_n}{U_t} \quad (9)$$

These relationships coupled with equation-of-state information of the form:

$$P = P(\mu) \quad (10)$$

serve to completely specify the impact situation under consideration. In the calculations to be discussed, experimental equation-of-state data for aluminum, magnesium, and beryllium were taken from Rice et al.^{13/}

The results of these calculations are presented in figures 13 through 16 in terms of ϕ as a function of pressure behind the shock front for fixed values of U_0 ranging from 7.5 mm/ μ sec to 15.0 mm/ μ sec. This velocity range corresponds roughly to the range of plate velocities, $V_p = U_0 \tan \phi$, achieved in conventional plate-throw experiments. It will be noted that for a given value of ϕ there are two solutions to the flow configuration corresponding to a weak and a strong shock situation. The weak shock solution associated with the lower values of pressure in figures 13 through 16 is the correct one. For a more complete explanation of this point see references 10 and 11. It will also be noted that no solution exists for beryllium at $U_0 = 7.5$ mm/ μ sec since this represents a subsonic flow configuration for this material under these conditions. The maximum values of ϕ in figures 13 to 16 correspond to the angle ϕ_c which delineates the jetless regime from the jetting situation for each value of U_0 . This is more conveniently illustrated in figure 17 where values of ϕ_c are plotted in terms of V_p , the plate velocity meas-

^{13/} Rice, M. H., R. G. McQueen, and J. M. Walsh. Compression of Solids by Strong Shock Waves. Solid State Physics, Vol. 6, Academic Press, Inc. (1958).

ured normal to its surface. As will be noted for aluminum, the use of the experimental equation of state leads to considerably different values of the parameters than were obtained in Walsh's original calculations. Other materials of interest are currently being treated and the results of these calculations will be reported when they become available.

TABLE 1. - Results of calibration trials using magnesium, aluminum, and brass attenuators.

Donor: 3/4-inch diam x 3/4-inch long tetryl ($\rho_0 = 1.57$)
Attenuator: 1-inch diam; thickness as specified
Wafer: 1/2-inch diam x 1/32-inch thick

| Thickness (in) | Recorded Time (μ sec) | Corrected Time (μ sec) | Wafer Velocity (mm/ μ sec) |
|--------------------------------------|-------------------------------|--------------------------------|-----------------------------------|
| <u>Magnesium (12.38 cm standoff)</u> | | | |
| 6/16 | 80.6 | 71.7 | 1.73 |
| 7/16 | 85.3 | 76.0 | 1.63 |
| 8/16 | 93.9 | 84.3 | 1.47 |
| 9/16 | 105.3 | 95.3 | 1.30 |
| 10/16 | 114.0 | 103.8 | 1.19 |
| <u>Aluminum (12.38 cm standoff)</u> | | | |
| 6/16 | 107.4 | 98.6 | 1.26 |
| 7/16 | 118.8 | 109.8 | 1.13 |
| 8/16 | 129.8 | 120.5 | 1.03 |
| 9/16 | 141.7 | 132.1 | 0.94 |
| 10/16 | 162.9 | 152.9 | 0.81 |
| <u>Brass (12.38 cm standoff)</u> | | | |
| 4/16 | 153.8* | 145.1 | 0.84 |
| 5/16 | 171.6 | 162.5 | 0.76 |
| 6/16 | 186.0 | 176.6 | 0.70 |
| 7/16 | 209.9 | 200.0 | 0.62 |
| 8/16 | 238.7 | 228.4 | 0.54 |

* Fired from a 12.14 cm standoff.

TABLE 2. - Data from streak photographs dealing with shock velocities in H₂O caused by spherical, pentolite charges.

| U_s (mm/ μ sec) | x (cm) | U_s (mm/ μ sec) | x (cm) |
|--------------------------|-----------|--------------------------|-----------|
| <u>Streak #72</u> | | | |
| Left Trajectory | | Right Trajectory | |
| 5.02 | 0.52 | 4.92 | 0.38 |
| 3.79 | 1.06 | 4.36 | 0.84 |
| 3.41 | 1.47 | 3.87 | 1.36 |
| 2.80 | 2.18 | 3.10 | 1.95 |
| 2.50 | 3.33 | 2.88 | 2.85 |
| 2.31 | 4.11 | 2.54 | 3.72 |
| 2.19 | 5.12 | 2.16 | 4.77 |
| 2.05 | 5.83 | 2.23 | 5.74 |
| -- | -- | 1.86 | 6.64 |
| <u>Streak #73</u> | | | |
| Left Trajectory | | Right Trajectory | |
| 4.44 | 0.20 | 4.65 | 0.30 |
| 3.33 | 0.54 | 3.51 | 0.70 |
| 2.86 | 0.94 | 3.33 | 1.15 |
| 2.49 | 1.44 | 2.96 | 1.71 |
| 2.40 | 2.54 | 2.70 | 2.85 |
| 2.40 | 3.59 | 2.40 | 3.98 |
| 2.29 | 4.66 | 2.11 | 4.98 |
| 2.19 | 5.64 | 2.15 | 5.92 |
| -- | -- | 2.04 | 6.86 |
| <u>Streak #74</u> | | | |
| Left Trajectory | | Right Trajectory | |
| 4.64 | 0.35 | 4.96 | 0.11 |
| 3.90 | 0.74 | 3.90 | 0.48 |
| 3.31 | 1.14 | 3.37 | 0.87 |
| 2.72 | 1.53 | 3.19 | 1.25 |
| 2.69 | 2.34 | 2.60 | 1.65 |
| 2.37 | 3.46 | 2.30 | 2.35 |
| 2.24 | 4.47 | 2.06 | 3.28 |
| 1.95 | 5.40 | 1.92 | 4.46 |
| 1.95 | 6.48 | -- | -- |

TABLE 2. - Data from streak photographs dealing with shock velocities in H₂O caused by spherical, pentolite charges
(cont'd).

| U_s (mm/ μ sec) | x (cm) | U_s (mm/ μ sec) | x (cm) |
|--------------------------|-----------|--------------------------|-----------|
| <u>Streak #75</u> | | | |
| Left Trajectory | | Right Trajectory | |
| 4.52 | 0.30 | 4.62 | 0.31 |
| 3.72 | 0.80 | 3.46 | 0.68 |
| 3.46 | 1.30 | 3.08 | 1.04 |
| 3.08 | 1.66 | 2.79 | 1.51 |
| 2.56 | 1.98 | 2.57 | 2.32 |
| 2.17 | 2.60 | 2.39 | 3.42 |
| 2.30 | 3.86 | 2.35 | 4.48 |
| 2.11 | 5.34 | 2.16 | 5.48 |
| -- | -- | 1.96 | 6.82 |
| <u>Streak #76</u> | | | |
| Left Trajectory | | Right Trajectory | |
| 5.33 | 0.44 | 4.80 | 0.31 |
| 3.52 | 1.01 | 3.52 | 0.80 |
| 2.96 | 1.37 | 2.68 | 1.20 |
| 2.75 | 1.62 | 2.62 | 1.78 |
| 2.45 | 2.29 | 2.49 | 3.16 |
| 2.32 | 3.37 | 2.46 | 4.24 |
| 2.15 | 4.35 | 2.37 | 5.31 |
| 2.07 | 5.30 | 2.24 | 6.34 |
| 1.86 | 6.17 | -- | -- |

TABLE 3. - Detonation rate data as a function of explosive diameter
for several explosive substances

| Diameter (in) | Wall Thickness (in) | Detonation Rate (mm/ μ sec) | | | |
|------------------|---------------------------|---|-----------------------------------|-------------------------------------|-------------------------------|
| | | INT (Cast)(c = 1.57) | Composition B (Cast)(c = 1.72) | 50/50 Pentolite (Cast)(c = 1.61) | 50/50 NG-EGDN (c = 1.55) |
| 0.237 | 0.039 | No detonation (n = 1) | 7.36 (n = 2) (E = 0.2%) | 7.16 (n = 2) (E = 0.3%) | 7.54 (n = 1) |
| 0.514 | 0.058 | No detonation (n = 2) | 7.83 (n = 4) (E = 0.3%) | 7.40 (n = 2) (E = 0.3%) | 7.52 (n = 2) (E = 0.0%) |
| 0.984 | 0.058 | 6.85 mm/ μ sec (n = 2) (E = 0.2%) | 7.82 (n = 2) (E = 0.0%) | 7.43 (n = 2) (E = 0.5%) | 7.51 (n = 2) (E = 0.2%) |
| 2.023 | 0.091 | 6.97 (n = 3) (E = 0.3%) | 7.89 (n = 2) (E = 0.2%) | 7.53 (n = 2) (E = 0.4%) | 7.54 (n = 2) (E = 0.5%) |

Notes: (1) n is the number of trials.

(2) E is the maximum percent deviation of any individual detonation rate from the average given.

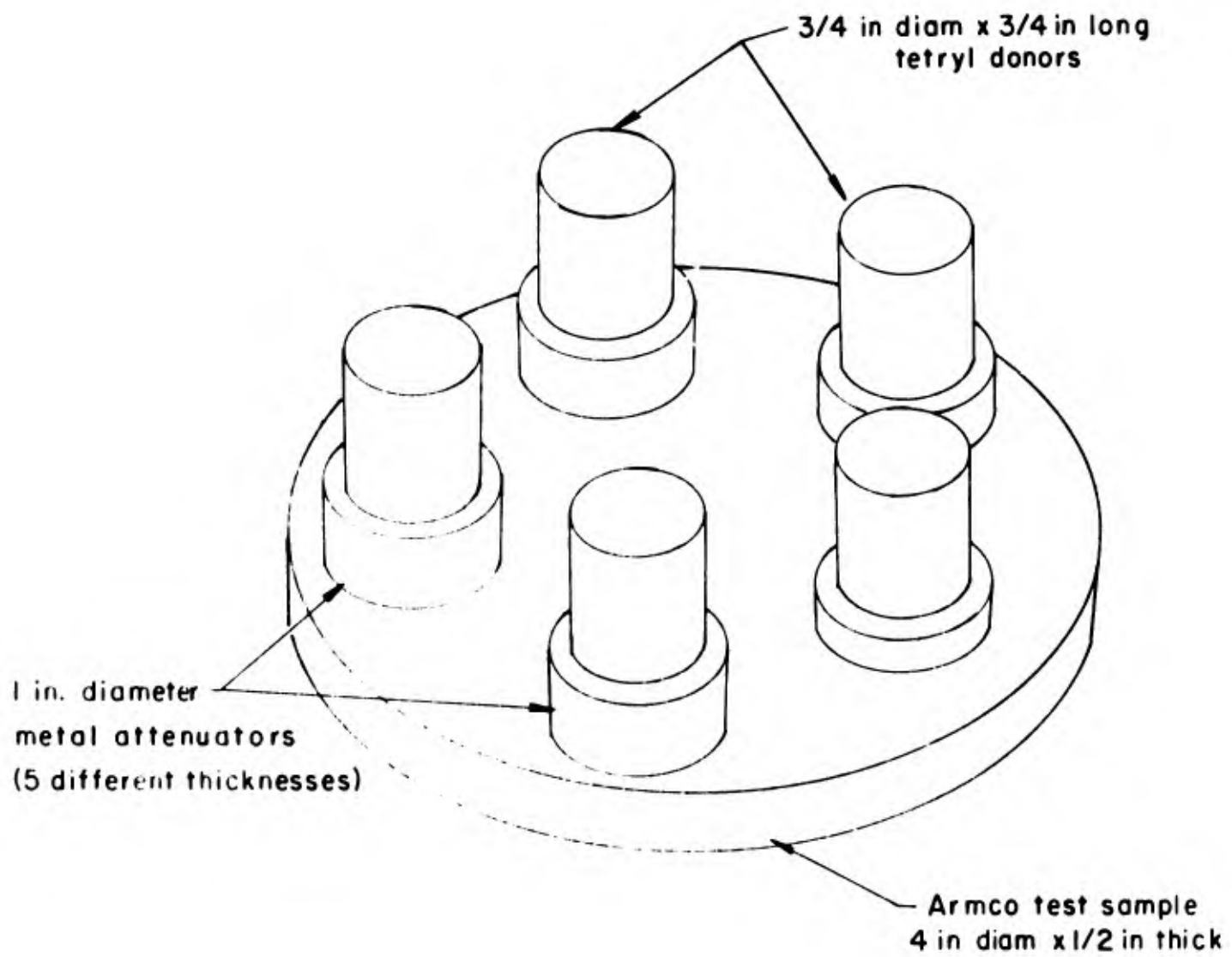


FIGURE 1. - Test arrangement used in shock wave signature studies.

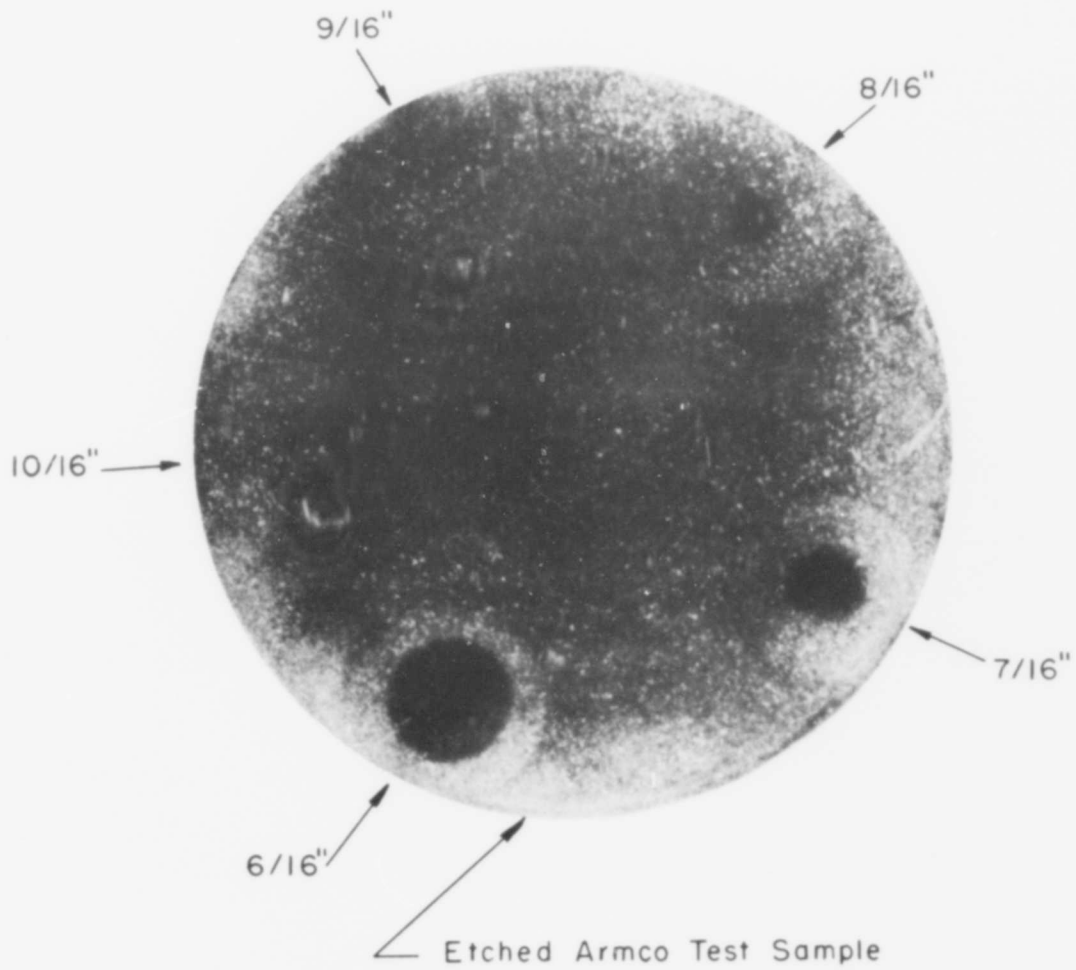


FIGURE 2. - Photograph of an etched Armco sample after shock loading with tetryl donors and aluminum attenuators.

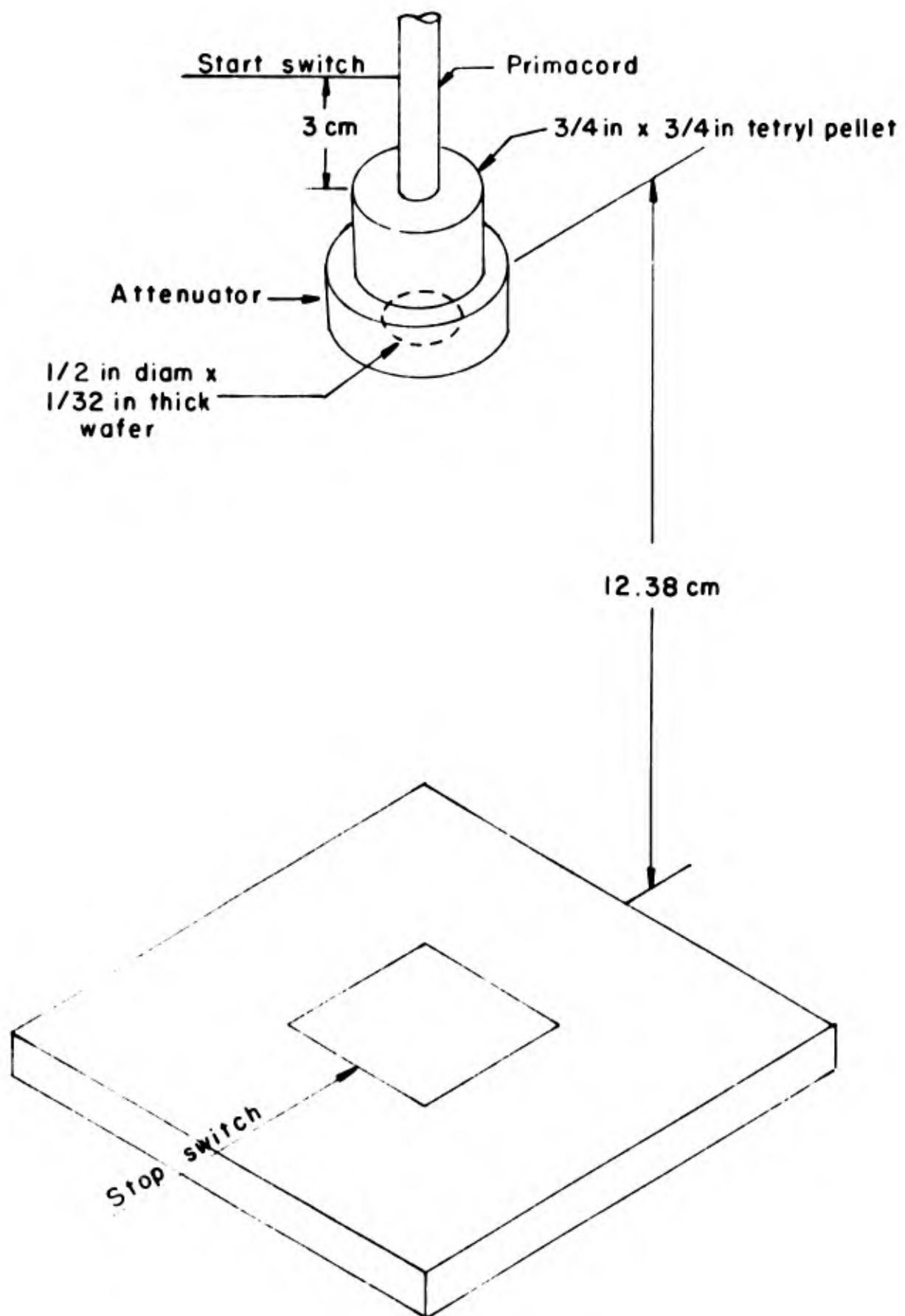


FIGURE 3. - Experimental arrangement used to calibrate the shock source used in signature studies with Armco iron.

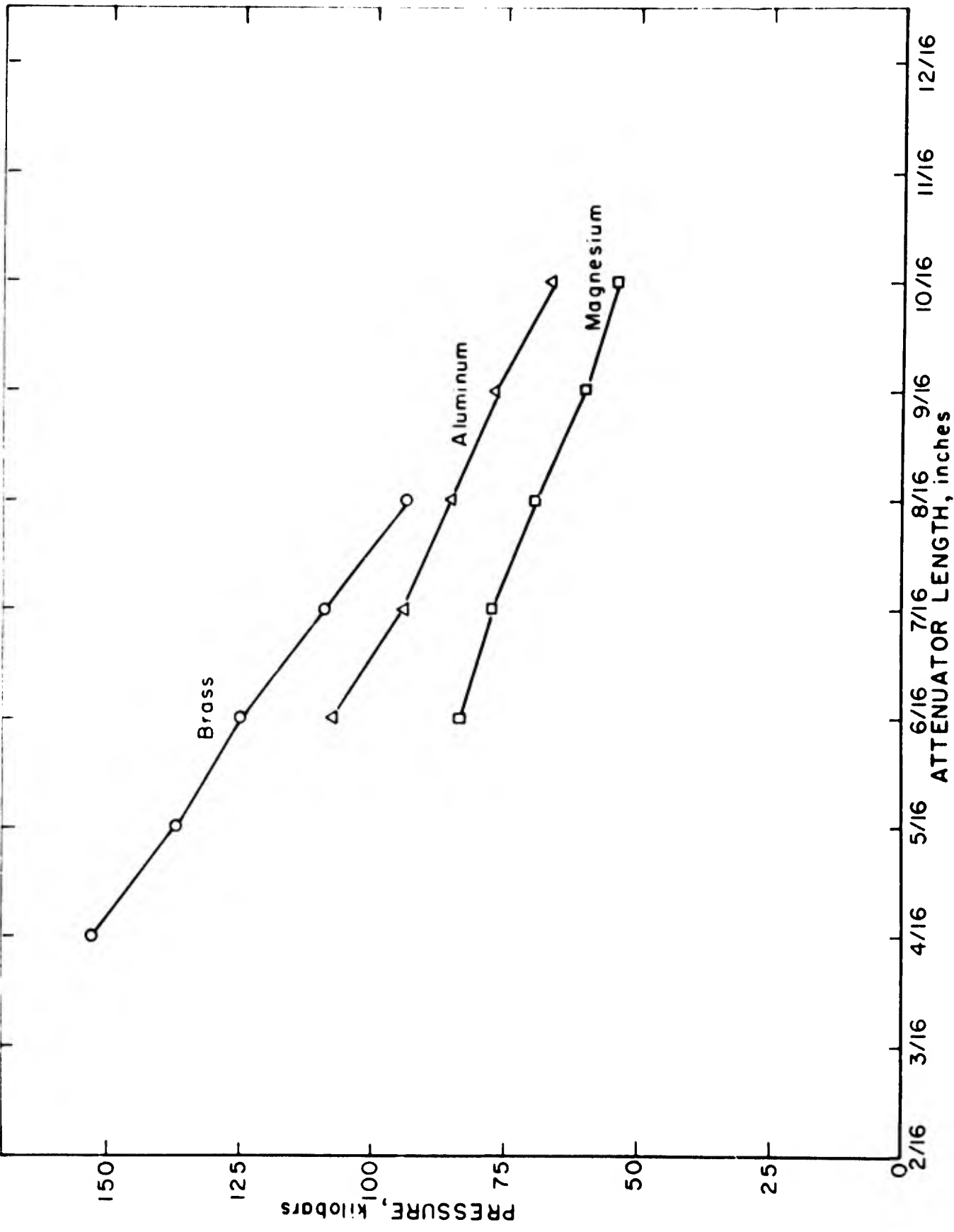


FIGURE 4. - Pressure as a function of attenuator thickness for three attenuator materials used in shock wave signature studies.

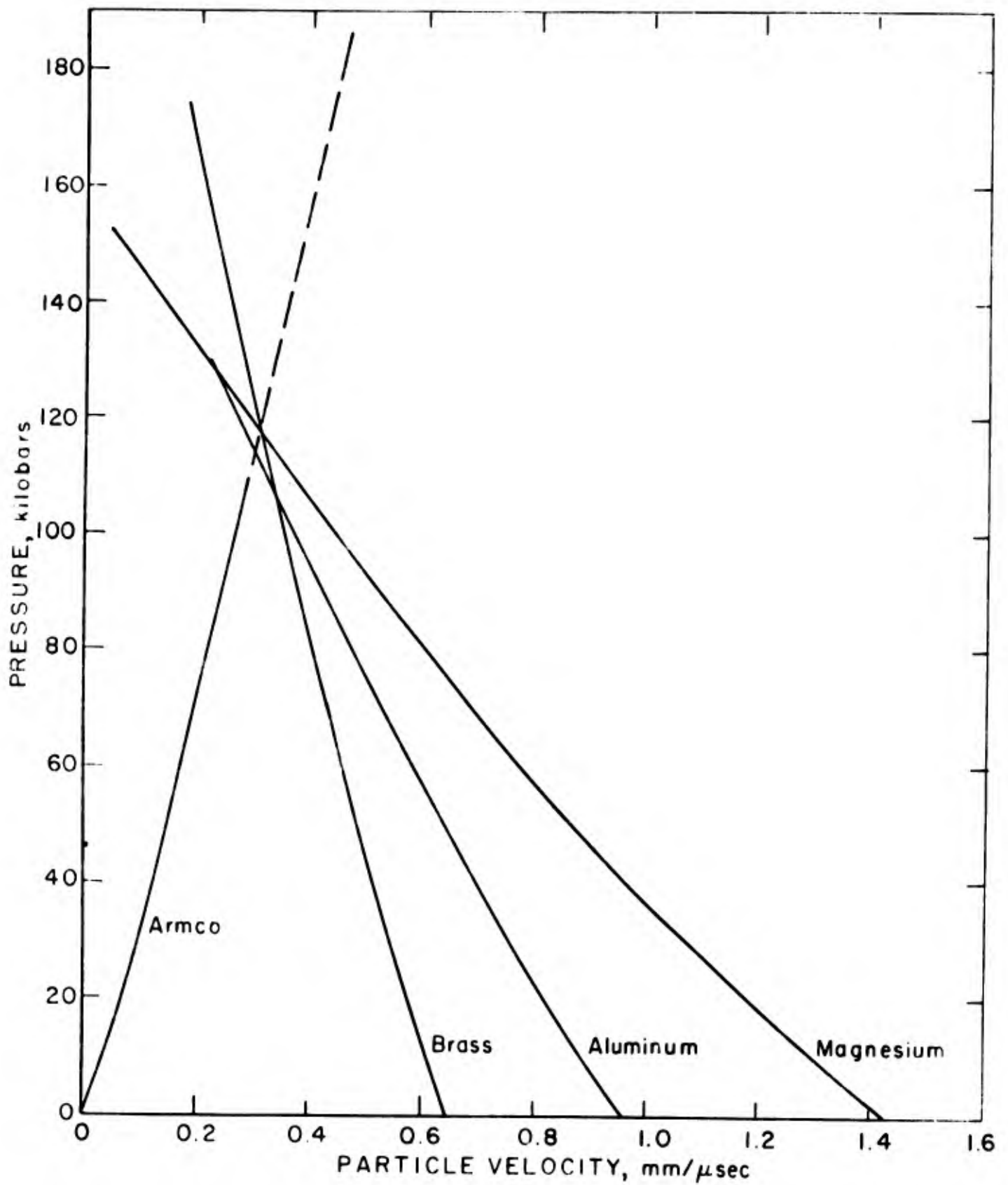


FIGURE 5. - Graphical solution for the common pressure delivered to Armco iron by three different donor-attenuator combinations.

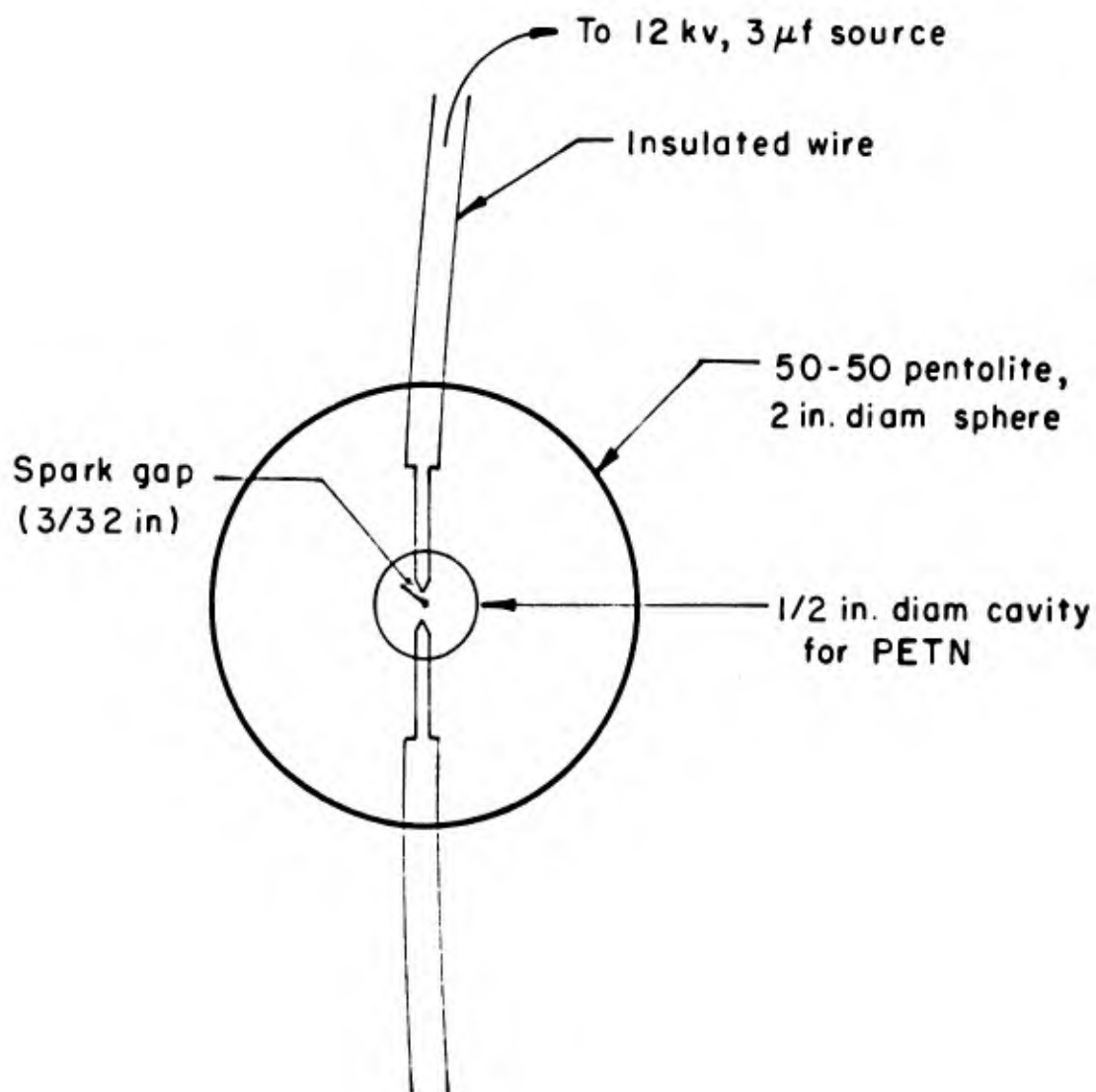


FIGURE 6. - Sketch of a 2-inch diameter spherical explosive charge and initiating mechanism.

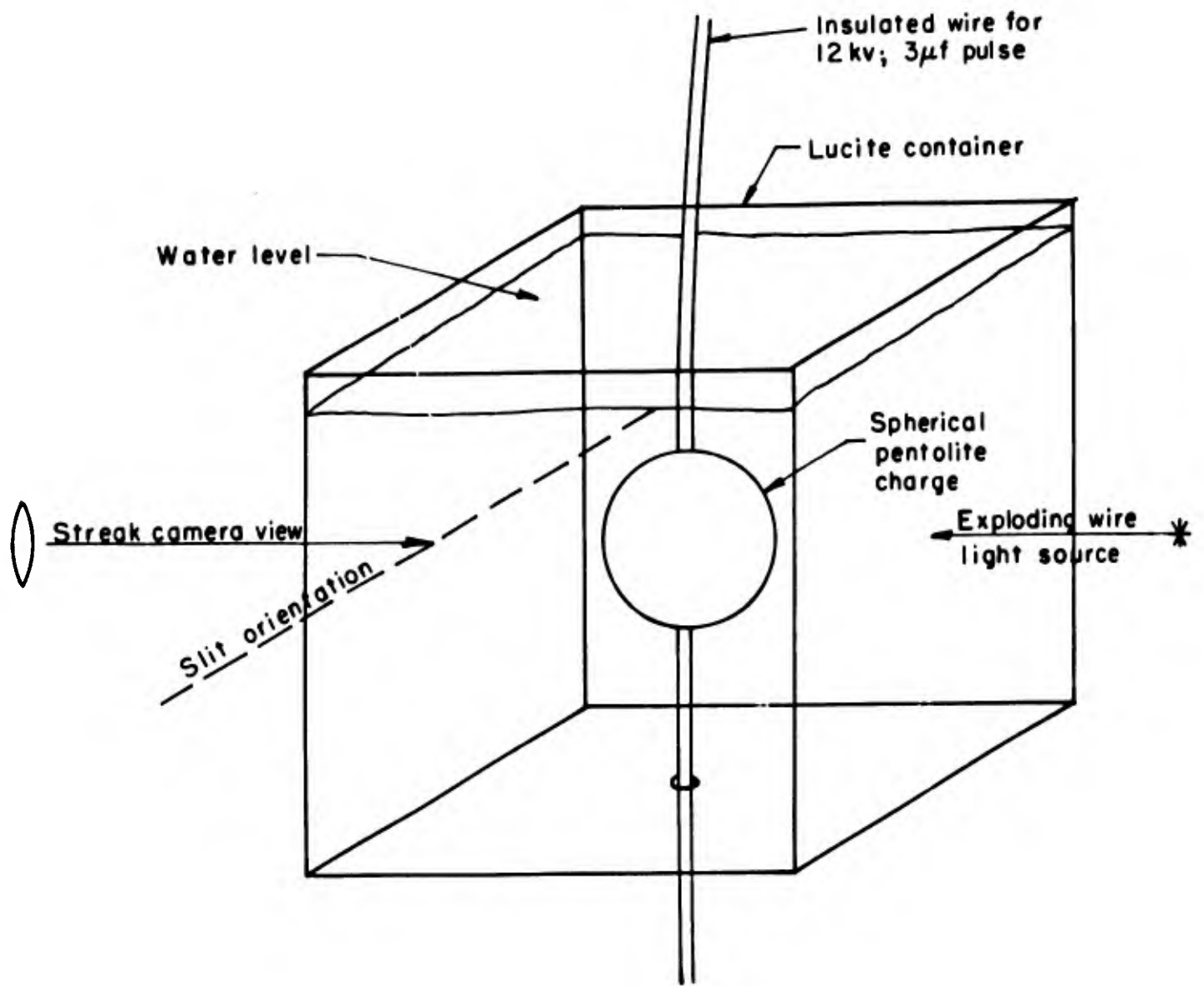


FIGURE 7. - Experimental arrangement used for spherical charge development work.

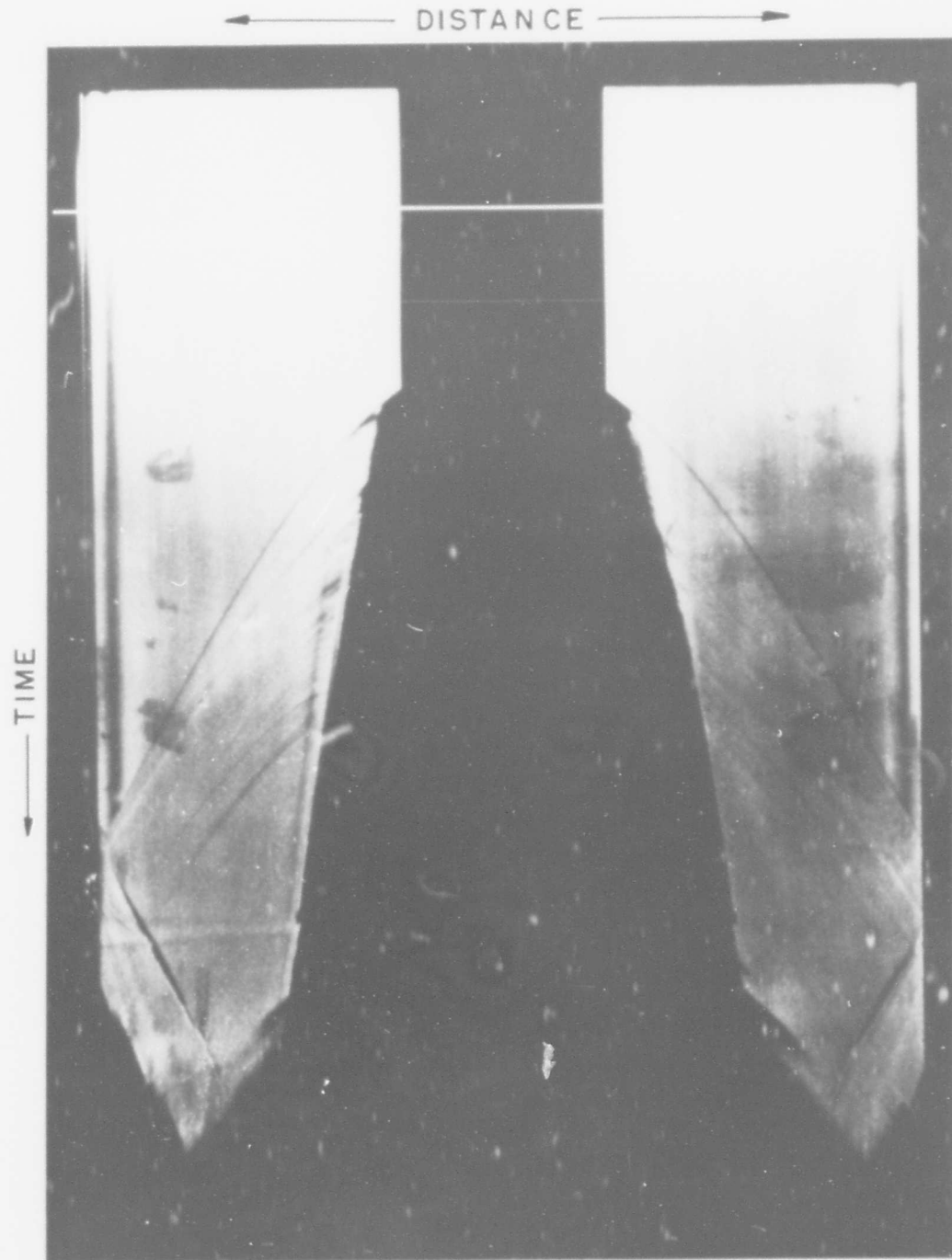


FIGURE 8. - Streak photograph of a shock wave from a spherical charge detonated in water.

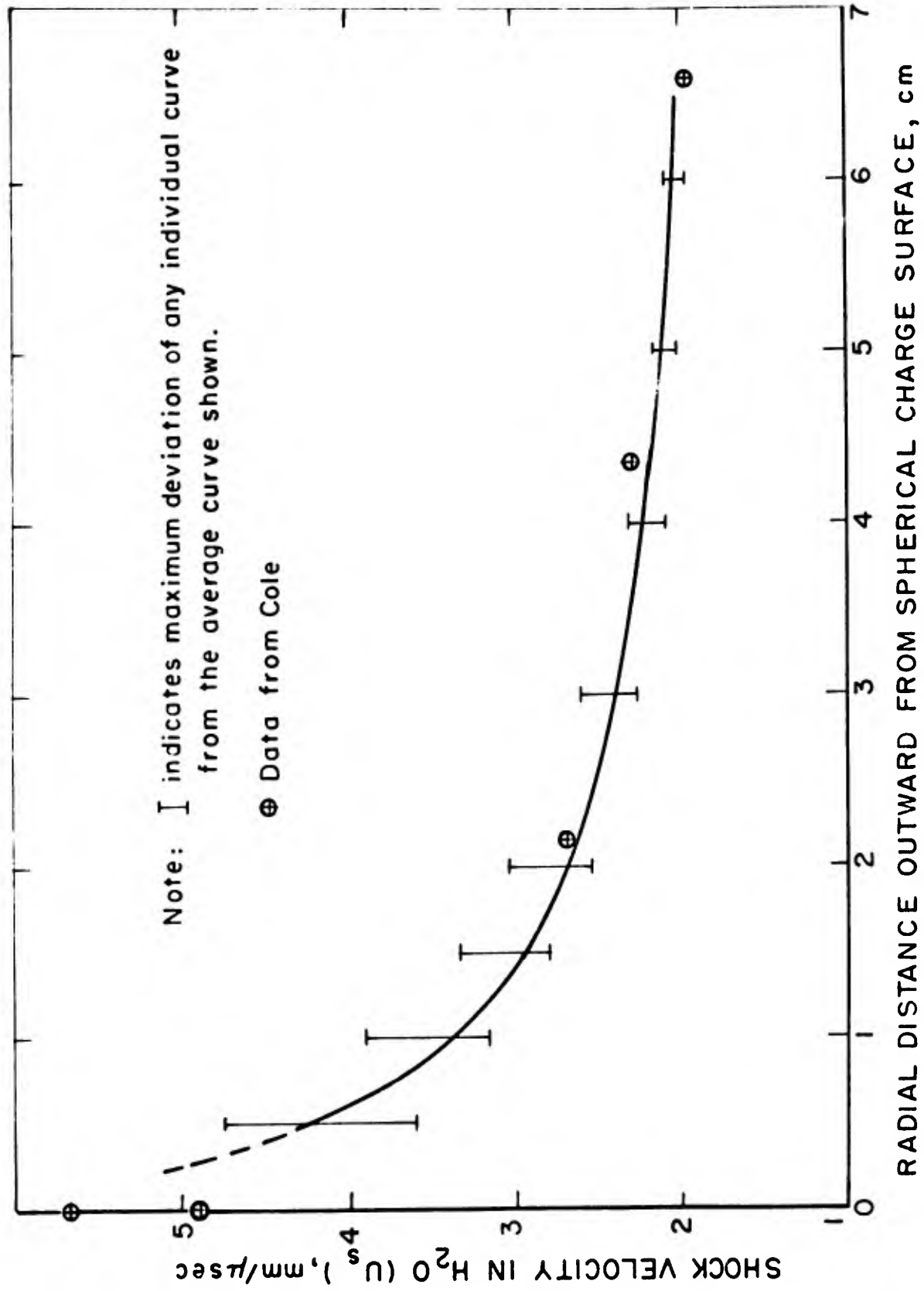
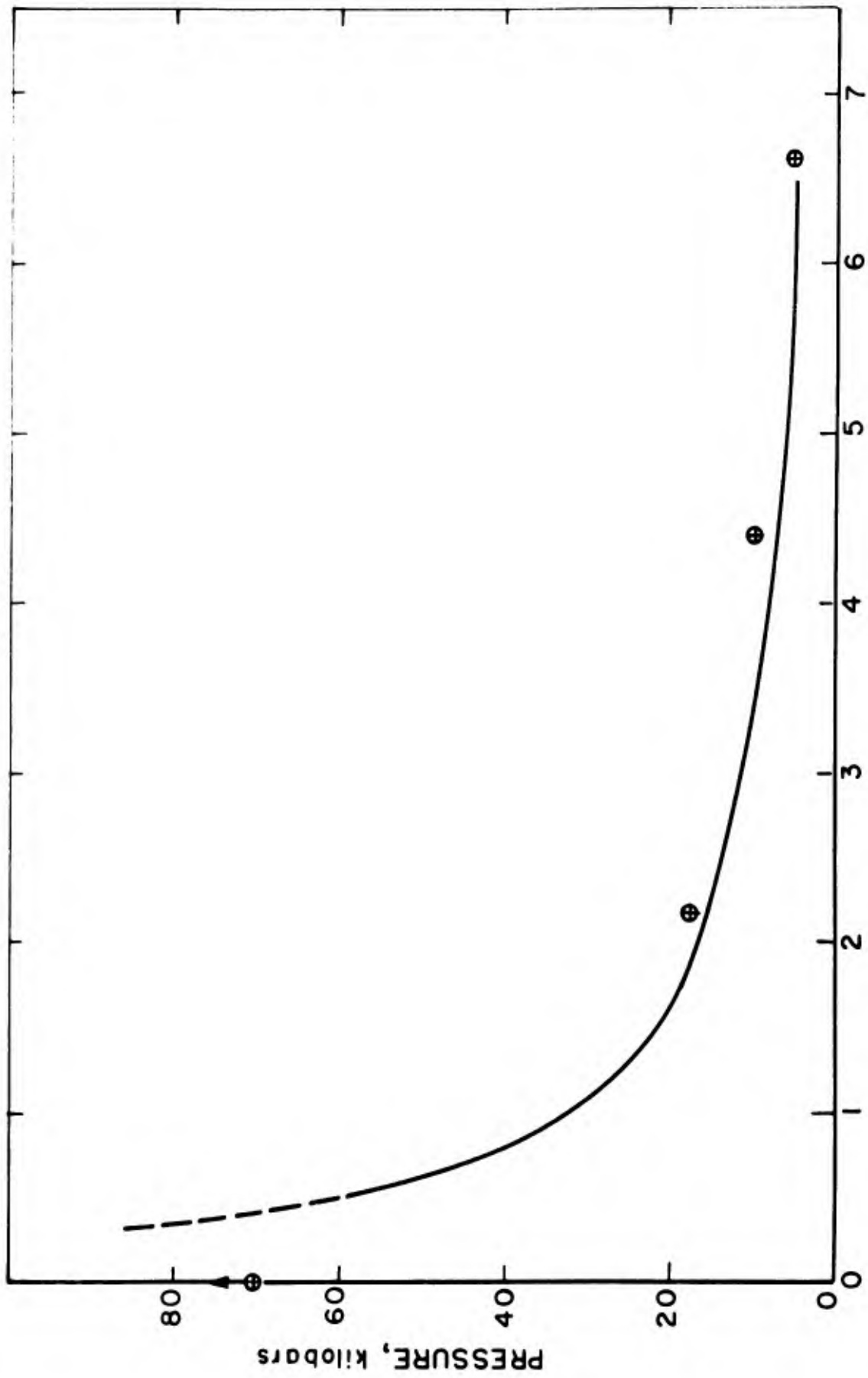


FIGURE 9. - Shock velocity versus radial position for spherical pentolite charges detonated under water.



RADIAL DISTANCE OUTWARD FROM SPHERICAL CHARGE SURFACE, cm

FIGURE 10. - Pressure versus radial position relationship for spherical pentolite charges detonated under water.

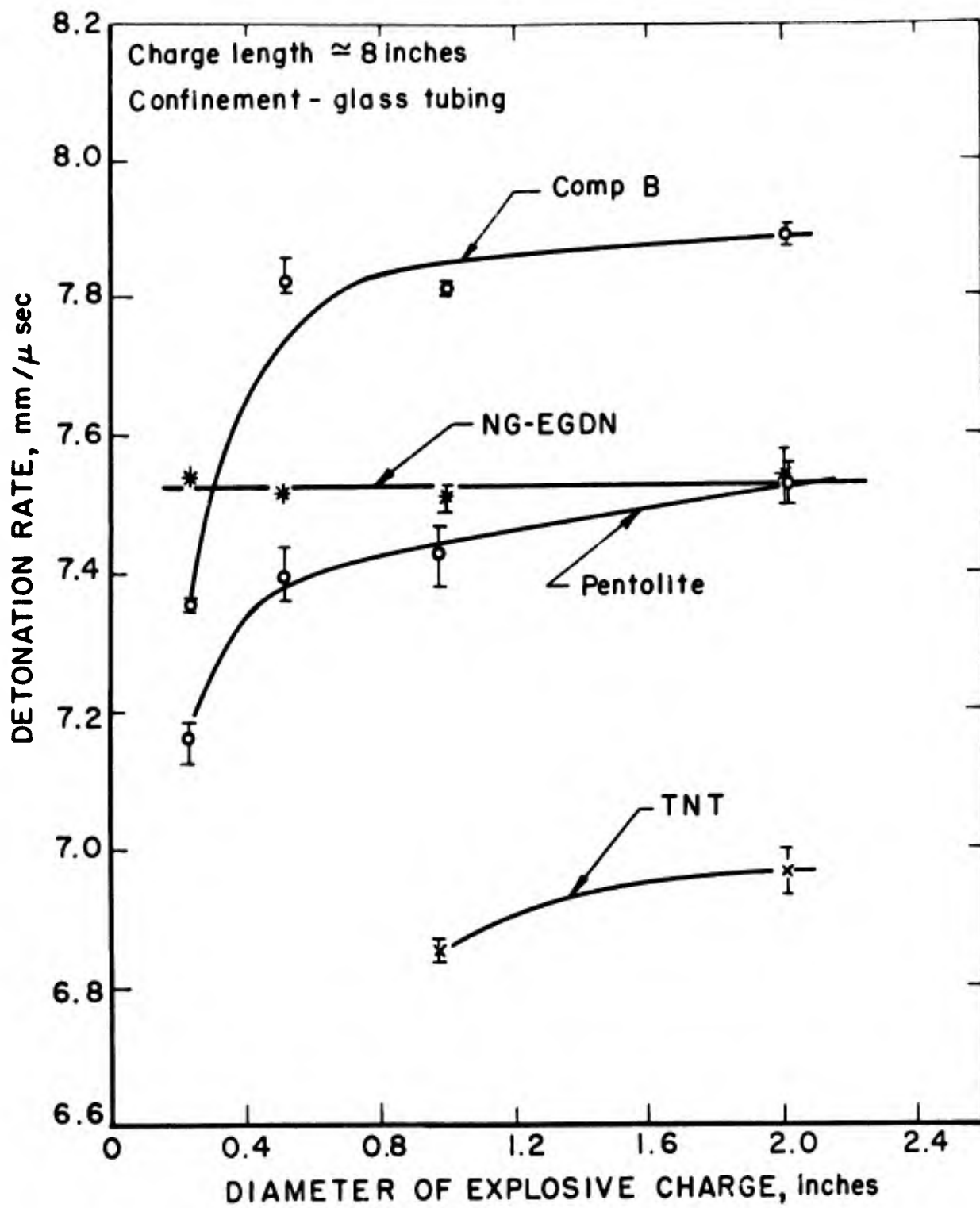


FIGURE 11. - Effect of explosive charge diameter upon detonation rate for several explosive substances.

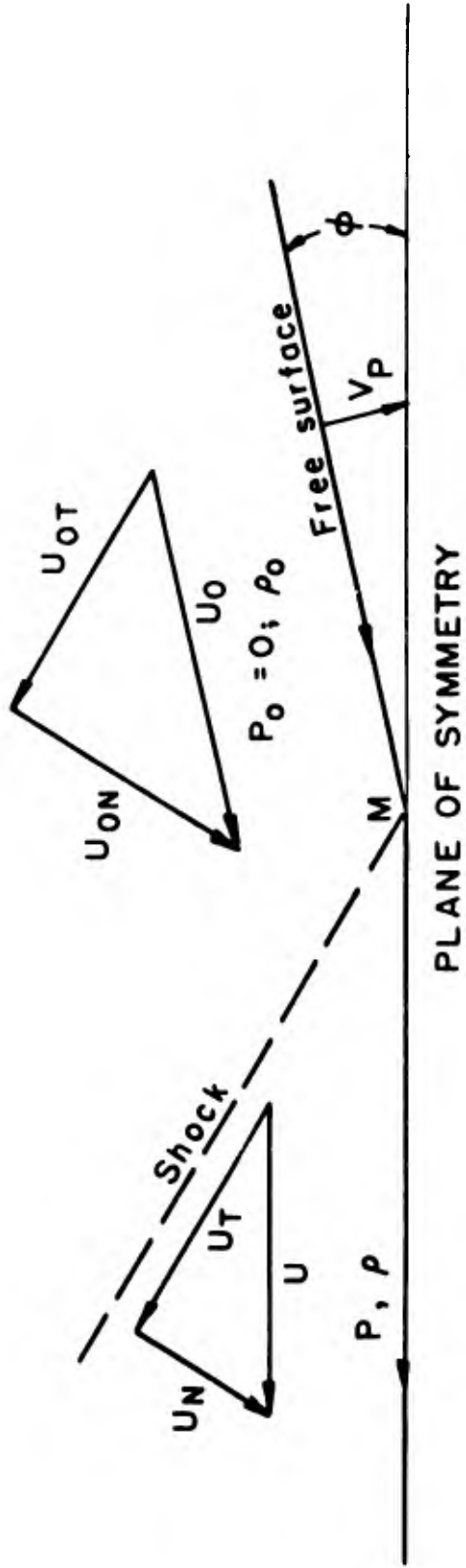


FIGURE 12. - Flow configuration for jetless collision of like materials.

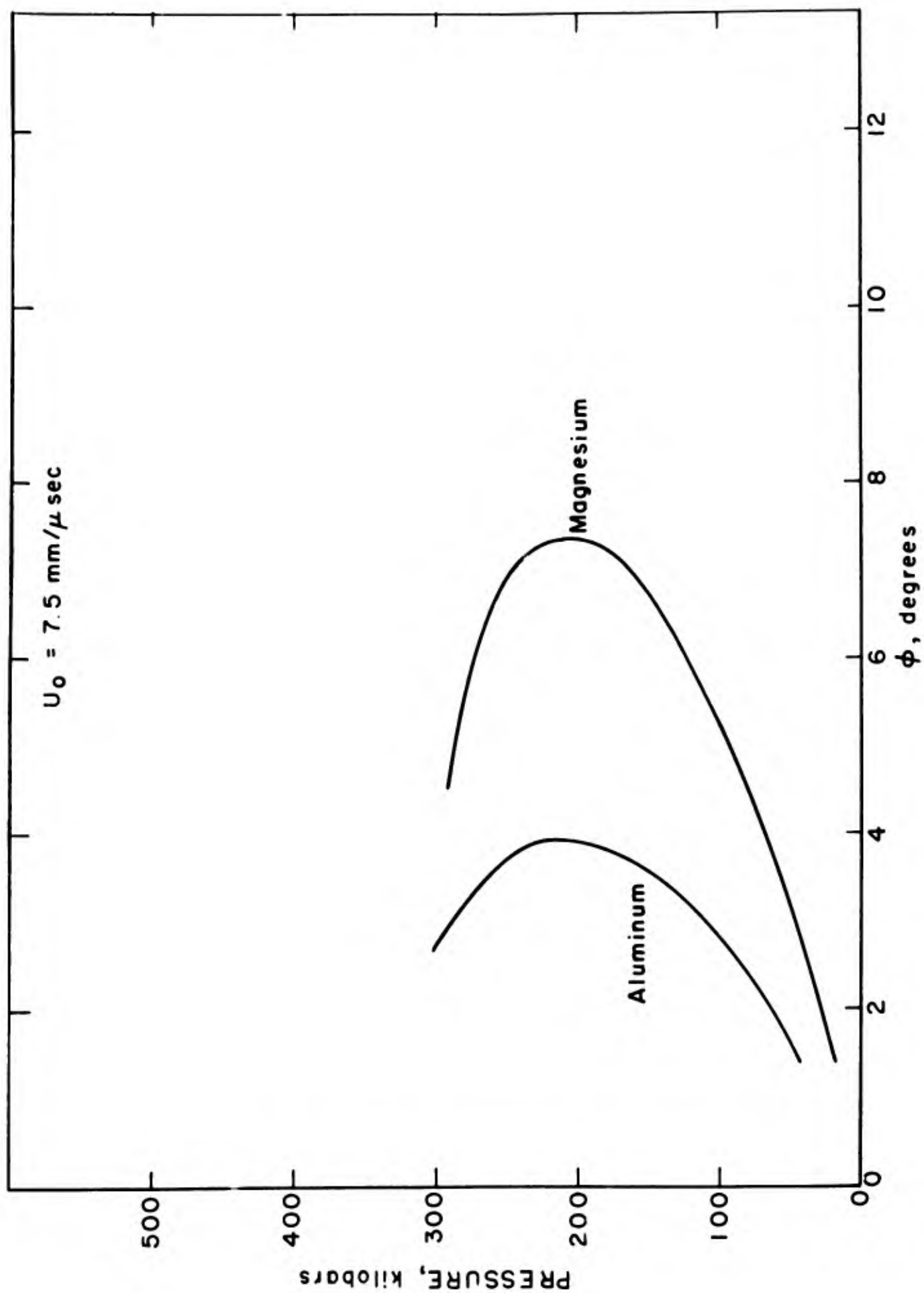


FIGURE 13. - ϕ versus P for aluminum and magnesium; $U_0 = 7.5 \text{ mm}/\mu\text{sec}$.

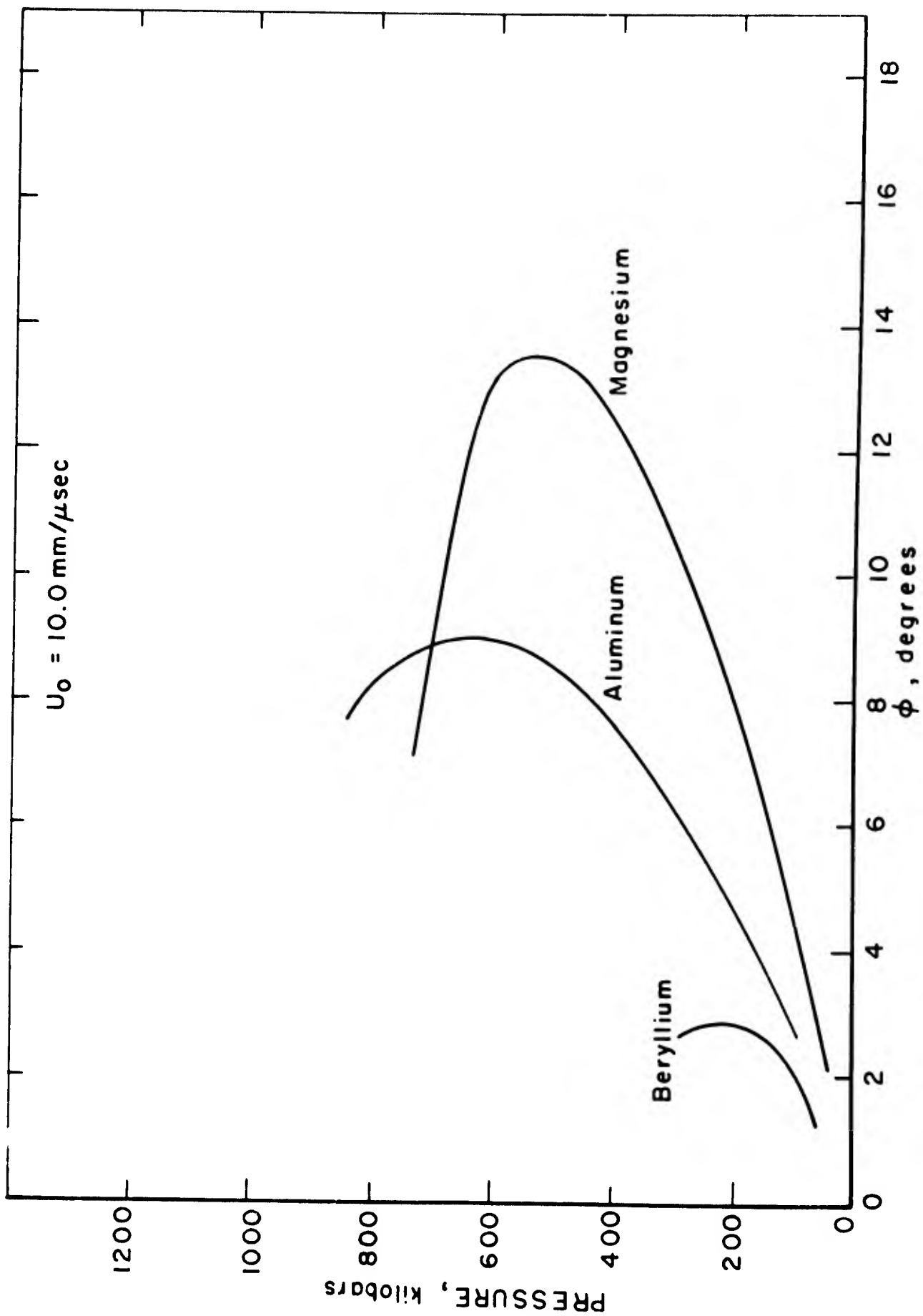


FIGURE 14. - ϕ versus P for aluminum, beryllium, and magnesium; $U_0 = 10.0$ mm/μsec.

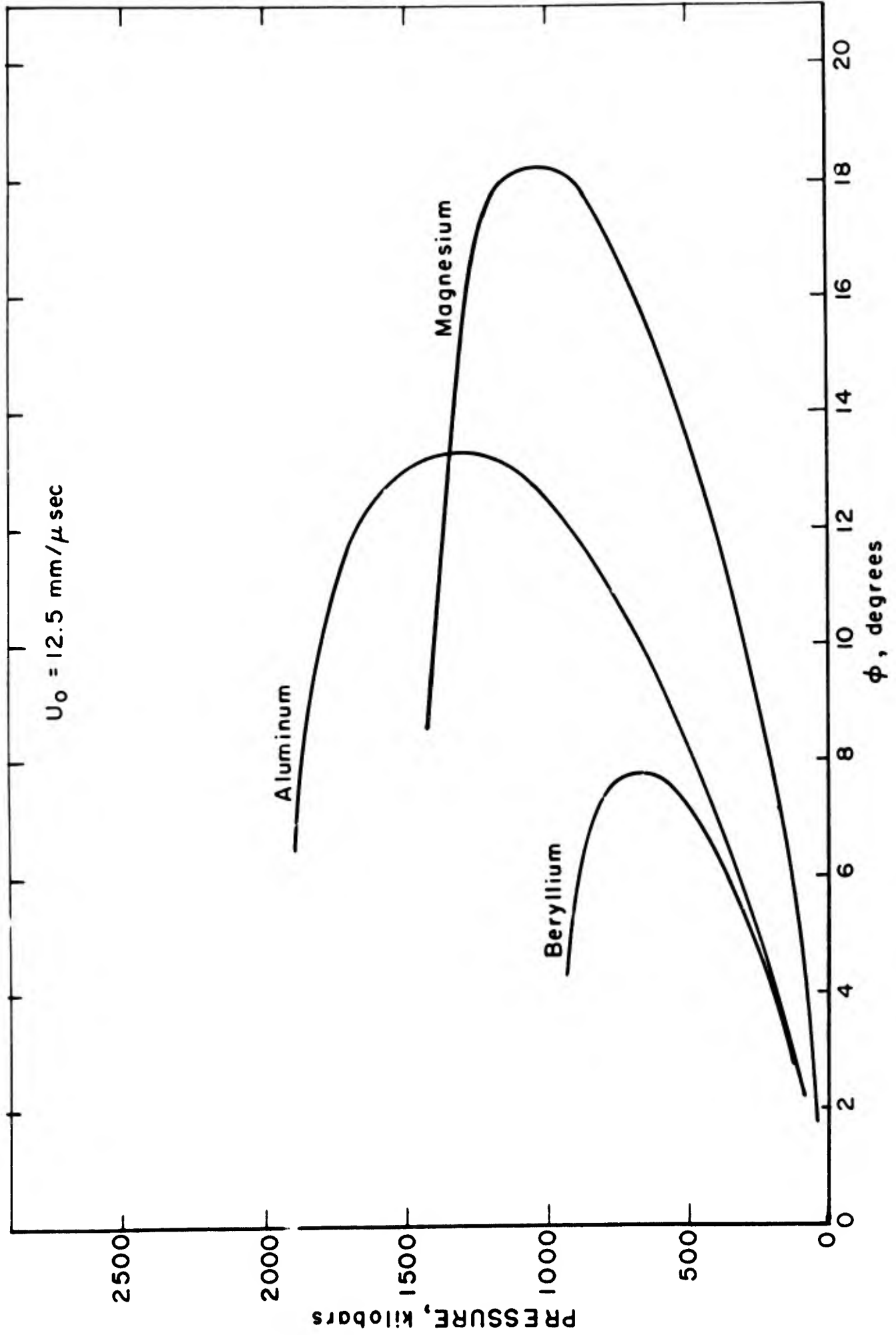


FIGURE 15. - ϕ versus P for aluminum, beryllium, and magnesium; $U_0 = 12.5 \text{ mm}/\mu\text{sec}$.

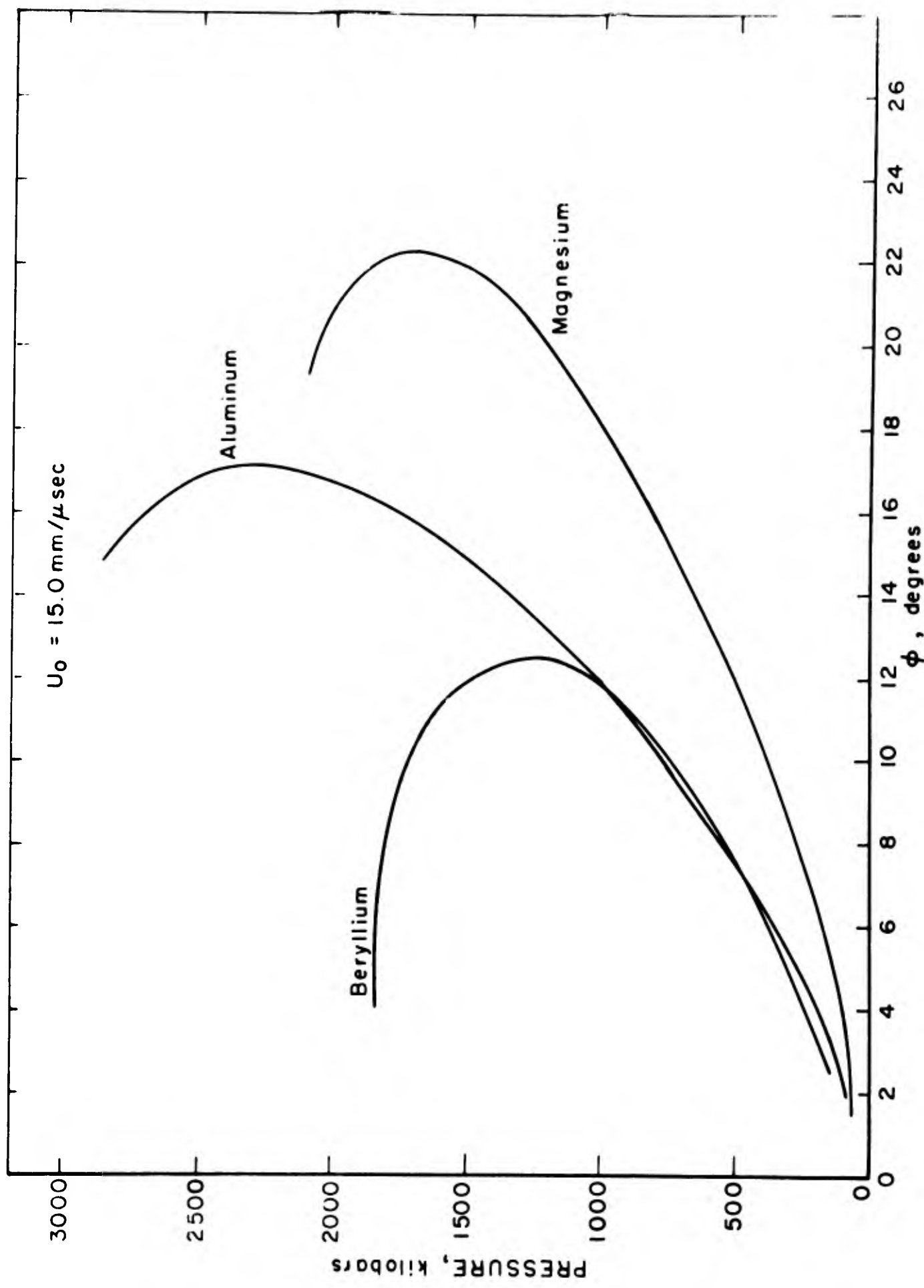


FIGURE 16. - ϕ versus P for aluminum, beryllium, and magnesium; $U_0 = 15.0 \text{ mm}/\mu\text{sec}$.

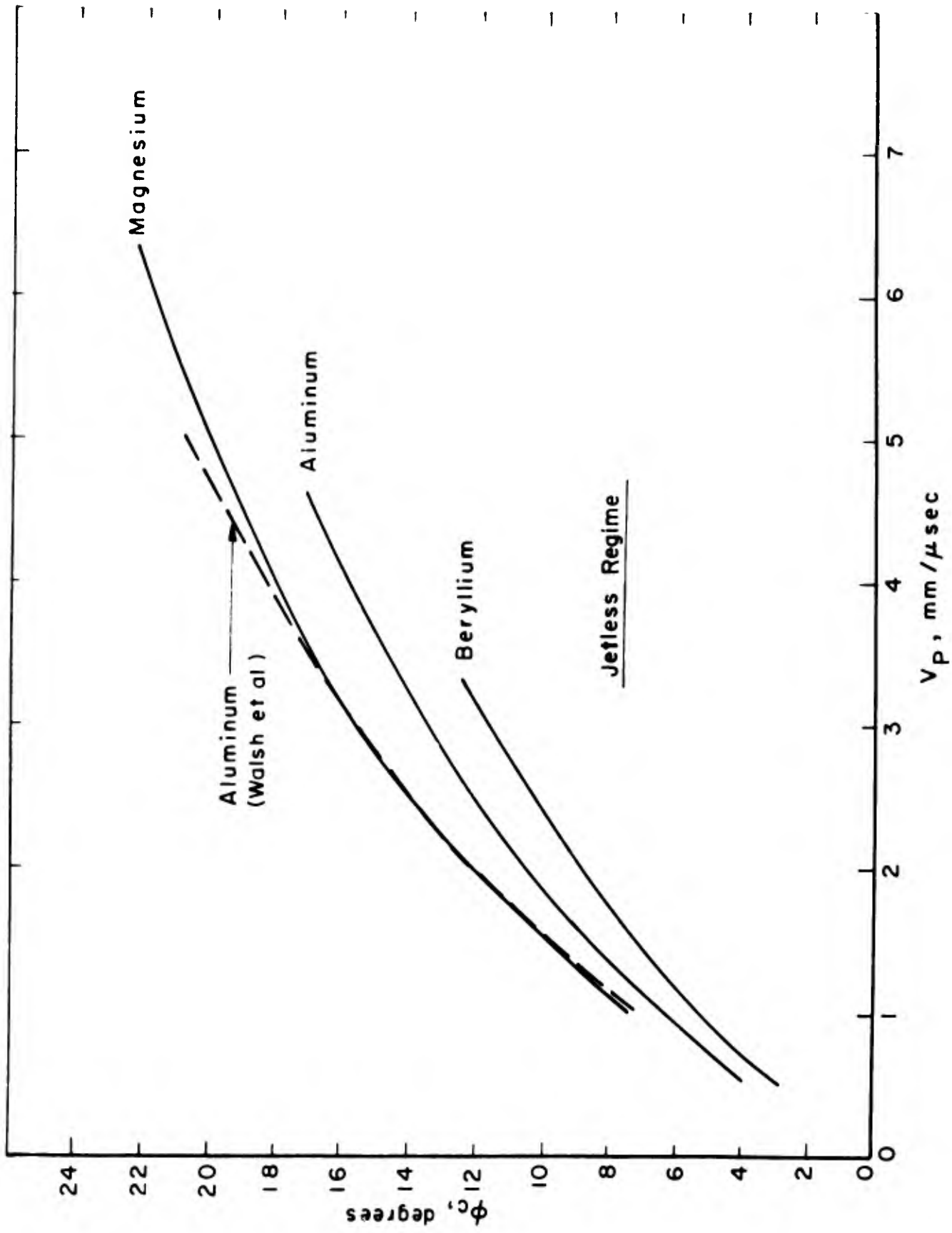


FIGURE 17. - ϕ_c versus V_p for aluminum, magnesium, and beryllium.